Tropical-Extratropical Interactions with the MJO Skeleton and Climatological Mean Flow

Shengqian Chen*

Department of Mathematics, University of Wisconsin–Madison, Madison, WI, USA.

Andrew J. Majda

Department of Mathematics, and Center for Atmosphere Ocean Sciences, Courant Institute of Mathematical Science, New York University, New York, New York, USA

Samuel N. Stechmann

Department of Mathematics and Department of Atmospheric and Oceanic Sciences, University of Wisconsin–Madison, Madison, WI, USA.

**Corresponding author address:* Shengqian Chen, Department of Mathematics, University of Wisconsin–Madison, Madison, WI, USA.

E-mail: sqchen@math.wisc.edu

ABSTRACT

Simplified asymptotic models are developed to investigate tropical–extratropical interactions. Two kinds of interactions are illustrated in the model: (i) MJO initiation through extraction of energy from the barotropic Rossby waves and (ii) MJO termination via energy transfer to extratropical Rossby waves. A new feature, in comparison to previous simplified models, is that here these waves interact directly in the presence of a climatological mean flow given by the Walker circulation. The simplified models are systems of ordinary differential equations (ODEs) for the amplitudes of barotropic Rossby waves and the MJO, and they are systematically derived from the MJO skeleton model by using multiscale asymptotics. The simplified ODEs allow for rapid investigation of a wide range of model parameters, such as initial conditions and wind shear. Background wind shear is shown to have only a minor effect on these interactions in the setup used here. The models illustrate some realistic features of tropical–extratropical interactions on intraseasonal to seasonal timescales. A key aspect of the models here is that the water vapor and convective activities are interactive components of the model, rather than specified external heating sources.

1. Introduction

The Madden-Julian Oscillation (MJO) is the dominant component of intraseasonal (≈30-60 days) variability in the tropics (Madden and Julian 1971, 1972, 1994). It is an equatorial wave envelope of complex multi-scale convective processes, coupled with planetary-scale (≈10,000-40,000 km) circulation anomalies. Individual MJO events propagate eastward at a speed of roughly 5 m/s, and their convective signal is most prominent over the Indian and western Pacific Oceans (Zhang 2005). In addition to its significance to its own right, the MJO also significantly affects many other components of the atmosphere-ocean-earth system, such as monsoon development, intraseasonal predictability in mid-latitude, and the development of the El Niño southern oscillation (ENSO) (Lau and Waliser 2012; Zhang 2005).

Besides its strong tropical signal, the MJO interacts with the global flow on the intraseasonsal timescales. Teleconnection patterns between the global extratropics and the MJO have been described in early observational analyses by Weickmann (1983), Weickmann et al. (1985) and Liebmann and Hartmann (1984). Their results demonstrate coherent fluctuations between extratropical flow and eastward-propagating outgoing longwave radiation (OLR) anomalies in the tropics. In a later study, Matthews and Kiladis (1999) illustrate the interplay between high-frequency transient extratropical waves and the MJO. More recently, Weickmann and Berry (2009) demonstrate that convection in the MJO frequently evolves together with a portion of the activity in a global wind oscillation. Gloeckler and Roundy (2013) argued by using lagged composite analysis that the high amplitude extratropical circulation pattern is associated with simultaneous assessment of both the MJO and the equatorial Rossby wave events.

Besides observational analyses, models have also been used to study the interactions between the MJO and extratropical waves. By including tropical convection forcing data in a model, Ferranti et al. (1990) found significant improvement in the model's predictability. Hoskins and Ambrizzi (1993) argued from their model that a zonally varying basic state is necessary for the MJO to excite extratropical waves by forcing perturbations to a barotropic model. To view the extratropical response to convective heating, Jin and Hoskins (1995) forced a primitive equation model with a fixed heat source in the tropics in the presence of a climatological background flow and obtain the Rossby wave train response as a result. To diagnose the more specific response to patterns of convection more like those of the observed MJO, Matthews et al. (2004) forced a primitive equation model in a climatological background flow with patterns of observed MJO. The resulting global response to that heating is similar in many respects to the observational analysis. The MJO initiation in response to extratropical waves was illustrated by Ray and Zhang (2010). They show that a dry-channel model of the tropical atmosphere developed MJO-like signals in tropical wind fields when forced by reanalysis fields at poleward boundaries. In addition, Lin et al. (2009) showed the significance of midlatitude dynamics in triggering tropical intraseasonal response by including extratropical disturbances in a tropical circulation model. Frederiksen and Frederiksen (1993) used a two-level primitive equation eigenvalue model and found that large-scale basic-state flow and cumulus heating to be necessary for generating MJO modes with realistic structures. Many other interesting studies on tropical–extratropical interactions have been carried out. For example, see the review by Roundy (2011).

Among the past studies based on climate models, typically the effect of the MJO is represented by forced perturbations (Hoskins and Ambrizzi 1993; Jin and Hoskins 1995; Matthews et al. 2004)or, the influence of the midlatitude variations are treated as boundary effects for the tropical circulation model (Ray and Zhang 2010; Lin et al. 2009; Frederiksen and Frederiksen 1993; Roundy 2011). Such simplifications are useful for isolating individual processes within these complex models. As a next step, it would be desirable to design a simplified model where both the

MJO and extratropical waves are simultaneously interactive, rather than externally imposing one of these two components.

Recently, a simplified model that includes the MJO and tropical-extratropical interactions was developed by Chen et al. (2015). This model combines the dry barotropic-first baroclinic interaction that has been studied by Majda and Biello (2003) and Khouider and Majda (2005) with (ii) the MJO skeleton model of Majda and Stechmann (2009, 2011). The MJO skeleton model includes the interactive dynamics of moisture q and convective activity envelope a. It has captured the main features of the MJO at the intraseasonal/planetary scale: (i) the slow phase speed of $\approx$5m/s, (ii) the peculiar dispersion relation of $\frac{\mathrm{d}\omega}{\mathrm{d}k} \approx 0$, and (iii) the horizontal quadrupole vortex structure. By combining the barotropic equations and the MJO skeleton, the model of Chen et al. (2015) illustrated applications to MJO initiation and termination, including three-wave interaction cases of (i) the MJO, equatorial baroclinic Rossby waves, and barotropic Rossby waves interacting, and (ii) the MJO, baroclinic Kelvin waves, and barotropic Rossby waves interacting. In those cases, the barotropic Rossby wave acts like a catalyst for the interaction between the MJO and dry equatorial waves, but its own amplitude is nearly unchanged. One of the main purposes of the present paper is to investigate scenarios where the barotropic Rossby waves may significantly exchange energy with the MJO. Two possible factors are wind shear and sea surface temperature (SST) variations and the accompanying variations in the climatological tropical circulation, the Walker circulation (Webster 1972, 1981, 1982; Hoskins and Jin 1991; Majda and Biello 2003). The present work will investigate the effects of regional varying SST and global shear flow in the interactions between the MJO and barotropic Rossby waves. It will be seen that the presence of the Walker circulation allows significant energy exchanges between barotropic Rossby waves and the MJO.

The paper is organized as follows. Section 2 describes the barotropic-first baroclinic MJO skeleton model, including SST regional variations and the resulting Walker circulation. Unbalanced moisture and cooling source terms with spatial variance are taken into account in the MJO skeleton to represent the effect of SST, in which case the Walker circulation can be found, that is, the steady state solution of the baroclinic system. The energy principle and asymptotic expansions are also presented. In Section 3, the resonance condition is identified in the presence of an idealized Walker circulation, which mediates the interaction between the MJO and the barotropic Rossby waves. Two cases are numerically computed for the ODE system: (i) MJO initiation, and (ii) MJO termination and excitation of barotropic Rossby waves. Section 4 considers more general Walker circulation cases composed of two different wave numbers. New ODE systems are derived for the resonant condition and numerical results are presented. Section 5 investigates the effect of a global shear flow. Finally, Section 6 is a concluding discussion.

2. Model description

a. The barotropic-first baroclinic MJO skeleton model

The barotropic-first baroclinic β-plane equations with water vapor and convection can be written as

$$\frac{\partial \overline{\mathbf{v}}}{\partial t} + \overline{\mathbf{v}} \cdot \nabla \overline{\mathbf{v}} + y \overline{\mathbf{v}}^{\perp} + \nabla \overline{p} = -\frac{1}{2} \nabla \cdot (\mathbf{v} \otimes \mathbf{v}), \tag{1a}$$

$$\nabla \cdot \overline{\mathbf{v}} = 0, \tag{1b}$$

for the barotropic mode, and

$$\frac{\partial \mathbf{v}}{\partial t} + \overline{\mathbf{v}} \cdot \nabla \mathbf{v} - \nabla \theta + y \mathbf{v}^{\perp} = -\mathbf{v} \cdot \nabla \overline{\mathbf{v}}, \tag{1c}$$

$$\frac{\partial \theta}{\partial t} + \overline{\mathbf{v}} \cdot \nabla \theta - \nabla \cdot \mathbf{v} = \delta^2 (\bar{H} a - S^{\theta}), \tag{1d}$$

$$\frac{\partial q}{\partial t} + \overline{\mathbf{v}} \cdot \nabla q + \tilde{Q} \nabla \cdot \mathbf{v} = -\delta^2 (\bar{H} a - S^{q}), \tag{1e}$$

$$\frac{\partial a}{\partial t} + \overline{\mathbf{v}} \cdot \nabla a = \Gamma q a. \tag{1f}$$

for the first-baroclinic mode. These equations combine the MJO skeleton model (Majda and Stechmann 2009) and nonlinear interactions between the baroclinic and barotropic modes (Majda and Biello 2003). The details of this model are described in Chen et al. (2015). Here $\overline{\mathbf{v}} = (\overline{u}, \overline{v})$ and $\overline{p}$ are barotropic velocity and pressure. The barotropic streamfunction ψ can be used to rewrite (1a)–(1b) as

$$\frac{\partial}{\partial t}\Delta\overline{\psi} + \overline{\mathbf{v}} \cdot \nabla\Delta\overline{\psi} + \psi_x + \frac{1}{2}\nabla \cdot [-(\mathbf{v}u)_y + (\mathbf{v}v)_x] = 0. \tag{2}$$

The other variables, $\mathbf{v} = (u, v)$ and θ are baroclinic velocity and potential temperature; and q is water vapor (sometimes referred to as "moisture"). The tropical convective activity envelope is denoted by $\delta^2 a$, where δ is a small parameter that modulates the scales of tropical convection envelope. We define δ^2 as the ratio of radiative cooling rate of 1 K/d divided by the reference heating rate scale at 10 K/day. Likewise, δ^2 is also incorporated with the quantities S^θ and S^q, radiative cooling and the moisture source. Here, for simplicity, we consider $\delta^2 S^\theta$ and $\delta^2 S^q$ to be spatially varying and time-independent, although in general, they have both spatial and temporal variations.

b. Walker circulation and energy evolution

First consider the baroclinic system (1c)–(1f) with the barotropic velocity ignored. When the system has unbalanced moistening and cooling sources, i.e., $S^q \neq S^\theta$, the Walker circulation is formed for the baroclinic equations with zero barotropic winds. When $\overline{\mathbf{v}} = 0$, the Walker circulation is the steady state solution for the baroclinic system (Ogrosky and Stechmann 2015):

$$\nabla\theta_{\mathrm{W}} + y\mathbf{v}_{\mathrm{W}}^{\perp} = 0, \tag{3a}$$

$$\nabla\cdot\mathbf{v}_{\mathrm{W}} = \delta^2\frac{S^\theta - S^q}{1-\tilde{Q}}, \tag{3b}$$

$$q_{\mathrm{W}} = 0, \tag{3c}$$

$$a_{\mathrm{W}} = \frac{S^q - \tilde{Q}S^\theta}{\bar{H}(1-\tilde{Q})}. \tag{3d}$$

When the Walker circulation variables are subtracted from the baroclinic variables, the baroclinic system has energy conservation for the anomalies: $\mathrm{d}\mathscr{E}_{\mathrm{BCa}}/\mathrm{d}t = 0$, where

$$\mathscr{E}_{\mathrm{BCa}} = \frac{1}{2}\int_{-Y}^{Y}\int_{0}^{X}\frac{1}{2}\left[|\mathbf{v}-\mathbf{v}_W|^2 + (\theta-\theta_W)^2\right] + \frac{1}{\tilde{Q}(1-\tilde{Q})}\left[q+\tilde{Q}(\theta-\theta_W)\right]^2 + \frac{\delta^2}{\tilde{Q}\Gamma}\left[\bar{H}a - a_W\log(a)\right]\mathrm{d}x\mathrm{d}y. \tag{4}$$

Now consider the full coupled system (1) including both the barotropic and baroclinic components. When the barotropic energy $\mathscr{E}_{\mathrm{BT}} = \frac{1}{2}\int_{-Y}^{Y}\int_{0}^{X}|\overline{\mathbf{v}}|^2\mathrm{d}x\mathrm{d}y$ is also considered, the total energy for the anomalies is $\mathscr{E} = \mathscr{E}_{\mathrm{BCa}} + \mathscr{E}_{\mathrm{BT}}$ and it evolves according to:

$$\begin{aligned}\frac{\mathrm{d}\mathscr{E}}{\mathrm{d}t} = -\frac{1}{2}\int_{-Y}^{Y}\int_{0}^{X} & \overline{\mathbf{v}}\cdot\nabla\left[\mathbf{v}_W\otimes\mathbf{v}_W + (\mathbf{v}-\mathbf{v}_W)\otimes\mathbf{v}_W + \mathbf{v}_W\otimes(\mathbf{v}-\mathbf{v}_W)\right] + (\mathbf{v}-\mathbf{v}_W)\cdot(\mathbf{v}_W\cdot\nabla\overline{\mathbf{v}} + \overline{\mathbf{v}}\cdot\nabla\mathbf{v}_W) \\ & + \left[\tilde{Q}q + (1+\tilde{Q}^2)(\theta-\theta_W)\right]\overline{\mathbf{v}}\cdot\nabla\theta_W\,\mathrm{d}x\mathrm{d}y.\end{aligned} \tag{5}$$

Note that the right-hand side of this equation is not zero, so the energy is not conserved.

c. Asymptotic ansatz

The asymptotic expansion is now carried out by introducing equatorial long-wave scaling,

$$x' = \delta x, \quad t' = \delta t, \quad \text{and} \quad v' = \frac{1}{\delta}v, \tag{6}$$

as well as the longer time scales:

$$T_1 = \delta t', \quad T_2 = \delta^2 t'. \tag{7}$$

Hence, in the asymptotic model, three long time scales are involved: t', T_1 and T_2. Their characteristic time scales are 1 day, 3 days and 10 days, respectively. In addition, small amplitude variables are also assumed for asymptotic expansion:

$$(\psi, u, v', \theta, q) = \delta^2(\psi_1, u_1, v_1, \theta_1, q_1) + \delta^3(\psi_2, u_2, v_2, \theta_2, q_2) + \delta^4(\psi_3, u_3, v_3, \theta_3, q_3) + O(\delta^5), \tag{8a}$$

and
$$a = \bar{a} + \delta a_1 + \delta^2 a_2 + \delta^3 a_3 + O(\delta^4), \tag{8b}$$

where each of the variables on the right-hand side of (8) is a function of x', t', T_1 and T_2, although this dependence has been suppressed in (8) to ease notation. For the moisture source and radiative cooling, it is assumed that

$$S^q = \overline{S^q} + \delta S^q{}_1, \qquad S^\theta = \overline{S^\theta} + \delta S^\theta{}_1, \tag{9}$$

where $\overline{\cdot} = \int \cdot \, \mathrm{d}x\mathrm{d}y$ is the mean value over the horizontal domain. We further assume that $\overline{S^q} = \overline{S^\theta} = \bar{H}\bar{a}$, which is a necessary consistency condition to ensure the existence of a steady Walker circulation (Majda and Klein 2003).

Under this assumption for S^q and S^θ, the Walker circulation would only appear in the leading order, so the baroclinic variables at the leading order can be written as:

$$[u_1, v_1, \theta_1, q_1, a_1] = [u_1, v_1, \theta_1, q_1, a_1]_{\mathrm{W}} + [u_1, v_1, \theta_1, q_1, a_1]_{\mathrm{a}} \tag{10}$$

where the subscript 'W' stands for Walker circulations, and the subscript 'a' stands for the leading order anomalies from the Walker circulation.

d. Meridional basis truncation

To carry out the multi-scale analysis, a meridional truncated basis is used for all of the variables. The main reason for introducing a meridional truncation is that the linear eigenmodes of (1) are not known, whereas the linear eigenmodes of a truncated version of this system are known and were previously described by Majda and Stechmann (2009). We adopt the same meridional structure described in Chen et al. (2015), where for the barotropic wind it is assumed that

$$\psi(x,y,t) = B(x,t)\sin(Ly), \tag{11}$$

where L is the meridional wavenumber. For the baroclinic variables, the meridional structures are assumed to be

$$l(x,y,t) = l^{(0)}(x,t)\Phi_0(y) + l^{(2)}(x,t)\Phi_2(y), \tag{12a}$$

$$r(x,y,t) = r^{(0)}(x,t)\Phi_0(y) + r^{(2)}(x,t)\Phi_2(y), \tag{12b}$$

$$v(x,y,t) = v^{(1)}(x,t)\Phi_1(y) \tag{12c}$$

$$q(x,y,t) = q^{(0)}(x,t)\Phi_0(y) + q^{(2)}(x,t)\Phi_2(y) \tag{12d}$$

$$\bar{H}a(x,y,t) - S^{\theta}(x,y,t) = \bar{H}a^{(0)}(x,t)\Phi_0(y). \tag{12e}$$

where $l = -\frac{u+\theta}{2}$ and $r = \frac{u-\theta}{2}$ are the Riemann invariants for the baroclinic system, and $\Phi(y)$ are the parabolic cylinder functions. The motivation for this particular truncation is mainly to have the simplest system that includes the Kelvin wave and the first symmetric equatorial Rossby wave; see Chen et al. (2015) for further discussion. The details of the parabolic cylinder functions can be found in the Appendix. In addition, we also assume that the variations for moisture source and radiative cooling share the same zonal structure:

$$S^{q}{}_{1} = \tilde{S}^{qy}(y)\tilde{S}^{x}(x), \quad S^{\theta}{}_{1} = \tilde{S}^{\theta y}(y)\tilde{S}^{x}(x), \tag{13}$$

although in general they often have different zonal structures. Further, the meridional structures are assumed to be proportional to the leading parabolic cylinder function:

$$\tilde{S}^{qy}(y) = c_q\Phi_0(y), \quad \tilde{S}^{\theta y}(y) = c_\theta\Phi_0(y), \tag{14}$$

The asymptotic expansions in (8) are then applied to the meridional truncated system, which is described in the Appendix. At the leading order, the truncated system is linear, and the baroclinic and barotropic systems are decoupled. The four major eigenmodes for the baroclinic system were described in Majda and Stechmann (2009), and they are the Kelvin, MJO, moist Rossby, and dry Rossby modes as shown in Figure 1.

3. Direct tropical-extratropical interaction mediated by Walker circulation

This section provides the reduced ODE model that includes direct tropical–extratropical interactions mediated by the Walker circulation. In particular, numerical computations for two cases will be given for this interaction mechanism: (i) MJO initiation and (ii) MJO termination and excitation of barotropic Rossby waves.

a. The reduced model

For the interaction of the MJO and barotropic Rossby wave, in the presence of the Walker circulation, their wave numbers and frequencies must satisfy the resonance condition:

$$k_{\mathrm{MJO}} + k_{\mathrm{W}} + k_{\mathrm{T}} = 0, \tag{15a}$$

$$\omega_{\mathrm{MJO}} + \omega_{\mathrm{T}} = 0 \tag{15b}$$

where k_{MJO}, k_{W} and k_{T} are the wave numbers for the MJO, the Walker circulation, and the barotropic Rossby wave, and ω_{MJO} and ω_{T} are the wave frequencies for the MJO and the barotropic Rossby wave. The frequency for the Walker circulation ω_{W} is zero. This type of resonance condition is analogous to topographic resonance (Majda et al. 1999). Because the MJO and barotropic Rossby waves travel in opposite directions, (15a) implies that the wavenumber of the Walker circulation has to satisfy the following condition:

$$|k_{\mathrm{W}}| \geq 2.$$

A Walker circulation with wavenumber $k_{\mathrm{W}} = 2$ can be viewed in Figure 2. One can view this wavenumber-2 Walker circulation as an idealization of the two main circulation cells in nature, which are centered over the maritime continent and South America (Stechmann and Ogrosky 2014; Ogrosky and Stechmann 2015). The resonance condition with $k_{\mathrm{MJO}} = 1$ and $k_{\mathrm{T}} = 1$ is shown in Figure 3.

To proceed with the multiscale analysis, we write the leading order baroclinic solution as

$$\vec{U}_1 = \alpha(T_1, T_2) e^{i(k_{\mathrm{MJO}} x - \omega_{\mathrm{MJO}} t)} \vec{r}_{\mathrm{MJO}} + \vec{r}_{\mathrm{W}} + \mathrm{C.C.}, \tag{16}$$

and the leading order barotropic solution as

$$B_1 = \frac{1}{\sqrt{2\pi L}} \beta(T_1, T_2) e^{i(k_{\mathrm{T}} x - \omega_{\mathrm{T}} t)} + \mathrm{C.C.}, \tag{17}$$

where C.C. stands for the complex conjugates, $\vec{r}_{\mathrm{MJO}}$ is the right eigenvector for the MJO mode, and $\vec{r}_{\mathrm{W}}$ is the right eigenvector of the Walker circulation. The eigenvector for the MJO mode is normalized by the baroclinic energy as described by Stechmann and Majda (2015).

Next, the second and third order systems are considered in order to determine the evolution of $\alpha(T_1, T_2)$ and $\beta(T_1, T_2)$ from (16) and (17) on the long time scales T_1 and T_2. A systematic multiscale asymptotic analysis is carried out to ensure the sub-linear growth of the second- and third-order terms of the asymptotic expansion in (8). Following similar procedures as in Chen et al. (2015), the result is a reduced ODE model for the amplitudes of the modes:

$$\partial_{T_2} \beta \qquad\qquad + i d_2 \beta + h_3 \alpha^* = 0, \tag{18a}$$

$$\partial_{T_2} \alpha + i d_4 \alpha^2 \alpha^* + i d_5 \alpha + h_6 \beta^* = 0, \tag{18b}$$

where coefficients ds and hs are pure real values and where $*$ denotes complex conjugate. Three groups of interacting terms appear in this ODE system: the cubic self-interaction term $id_4\alpha^2\alpha^*$ corresponding to the nonlinear q-a interaction, the linear self-interaction terms $id_2\beta$ and $id_5\alpha$ related to dispersive terms in the barotropic-baroclinic system, and the coupled linear terms $h_3\alpha^*$ and $h_6\beta^*$ related to the Walker circulation. In contrast to the ODE system derived by Chen et al. (2015) where the coupling terms are quadratic, here the coupling terms $h_3\alpha^*$ and $h_6\beta^*$ are linear. This is because the Walker circulation is involved in this coupling, but it is a stationary mode with fixed amplitude, so that one part of the quadratic term is a fixed value.

The values of h_3 and h_6 in (18) are determined by the strength of the variations in the source terms, ${S^q}_1$ and ${S^\theta}_1$, or their meridional projection coefficients c_q and c_θ from (14), as is shown in Table 1. In this paper, for simplicity, the two coefficients are fixed so that $c_q = 1.2$ and $c_\theta = 1$, which results in the Walker circulation shown in Figure 2.

According to (18), the coupled linear terms determine the energy exchange between the two modes:

$$\frac{\mathrm{d}|\alpha|^2}{\mathrm{d}T_2} = -2h_3\mathrm{Re}(\alpha\beta), \quad \frac{\mathrm{d}|\beta|^2}{\mathrm{d}T_2} = -2h_6\mathrm{Re}(\alpha\beta), \tag{19}$$

where Re denotes the real part. At the leading order, the total energy E for the anomalies is

$$E = |\alpha|^2 + |\beta|^2, \tag{20}$$

which is only conserved when $h_3 + h_6 = 0$. However, this is generally not the case. In Table 1, h_3 and h_6 have opposite signs, indicating from (19) that as one mode is gaining energy, the other one is losing energy, but the total energy is not necessarily constant.

Here the simplified asymptotic equations in (18) are utilized to gain insight into the interactions between the MJO and the barotropic Rossby waves. For this purpose, the reduced model is integrated numerically for two sets of initial data: (i) MJO initiation: $\alpha|_{T_2=0} = 0$ and $\beta|_{T_2=0} = 1$, and

(ii) MJO termination and excitation of barotropic Rossby waves: $\alpha|_{T_2=0} = 1$ and $\beta|_{T_2=0} = 0$. The computation time is up to 200 days to observe the properties of the solutions on the long T_2 time scale. A standard fourth-order Runge-Kutta time discretization is adopted as the basic numerical method. The accuracy of the numerical solution is checked by doubling and halving the time-steps and ensuring the relative difference between these solutions at 200 days is within 0.1 %.

b. MJO initiation

To simulate a case of MJO initiation, the initial conditions are set to be $\alpha|_{T_2=0} = 0$ and $\beta|_{T_2=0} = 1$. From the reduced model (18), it can be seen that the nonzero value of β will excite α through the coupled linear terms. The numerical simulation in Figure 4 shows this behavior initially where the MJO gains energy while the barotropic Rossby wave is losing energy, and the total energy is increasing until it peaks at around 70 days. After this time, the MJO mode decays in amplitude as the barotropic Rossby wave gains energy and returns to the original state. This patterns repeats itself to be a nonlinear cycle with time period of roughly 140 days.

To illustrate the spatial variations, Figure 5 shows the Hovmoller diagram for $\bar{H}a_{1\mathrm{a}}$, the leading order anomaly of the convective activity. In this figure, the MJO is traveling eastward at a speed of $\sim$5 m/s, and the wave amplitude is zero at 0 day, peaks at around 70 day, and returns back to zero-amplitude at 140 day. This corresponds to a wave train of roughly one or two MJO events, depending on the spatial location, similar to the organization of sequences of MJO events in nature (Yoneyama et al. 2013; Thual et al. 2014). In Figure 6, the horizontal velocity fields at lower-troposphere are shown for the MJO, the barotropic Rossby wave and the Walker circulation. The Walker circulation is a stationary field. For the MJO, the velocity field is zero at 0 day, and achieves its maximum at 70 day. The barotropic Rossby wave is at its maximum initially, and achieves its smallest magnitude at 70 day.

c. MJO termination and excitation of barotropic Rossby waves

To consider MJO termination and the excitation of barotropic Rossby waves, the initial condition is set to be $\alpha|_{T_2=0} = 1$ and $\beta|_{T_2=0} = 0$. Figure 7 shows the numerical simulation from the ODE solver. In this case, at the initial time, the MJO is losing energy whereas the barotropic Rossby wave is gaining energy, and the total energy of these two modes are decaying at first, until $\sim$70 day. The amplitudes and energy return to their original state at around 140 day.

4. More general Walker circulation

In the previous section, the case for the sinusoidal Walker circulation with wavenumber $k_{\mathrm{W}} = 2$ is discussed. The realistic Walker circulation, on the other hand, is composed of a variety of wave numbers. For example, Ogrosky and Stechmann (2015) described simplified versions of the Walker circulation using 1 or 3 Fourier modes in their study. In this section, another mode for the Walker cell, $k_{\mathrm{W}} = 3$ is also included in addition to $k_{\mathrm{W}} = 2$. The Walker circulation in this case is shown in Figure 8. In this situation, two sets of resonant triads arise corresponding with the two Walker cell wavenumbers:

$$k_{\mathrm{MJO}1} + k_{\mathrm{W}1}(=-2) + k_{\mathrm{T}1} = 0, \tag{21a}$$

$$\omega_{\mathrm{MJO}1} + \omega_{\mathrm{T}1} = 0, \tag{21b}$$

and

$$k_{\mathrm{MJO}2} + k_{\mathrm{W}2}(=-3) + k_{\mathrm{T}2} = 0, \tag{22a}$$

$$\omega_{\mathrm{MJO}2} + \omega_{\mathrm{T}2} = 0. \tag{22b}$$

To select some reasonable cases for illustration, the values for $k_{\mathrm{MJO}1}$ and $k_{\mathrm{T}1}$ are both fixed to be 1, and two cases are considered: (i) $k_{\mathrm{MJO}2} = 1$, $k_{\mathrm{T}2} = 2$, and (ii) $k_{\mathrm{MJO}2} = 2$, $k_{\mathrm{T}2} = 1$. For case (i), $k_{\mathrm{MJO}1}$ and $k_{\mathrm{MJO}2}$ represent the same $k=1$ MJO mode. For case (ii), $k_{\mathrm{T}1}$ and $k_{\mathrm{T}2}$ are the same wavenumber, but they represent barotropic Rossby waves with different meridional wavelengths. In the two cases below, the strength of ${S^{\theta}}_1$ and ${S^{q}}_1$ at wavenumber $k=3$ are also chosen to be $c_q=1.2$ and $c_\theta=1$, as in the previous section, for simplicity, although more general situations can be applied.

a. MJO–b.t. Rossby–b.t. Rossby

Here three modes are considered: the MJO mode with wavenumber $k_{\mathrm{MJO}1}=1$, the barotropic Rossby waves with $k_{\mathrm{T}1}=1$ and $k_{\mathrm{T}2}=2$. The resonance conditions for the three modes are shown in Figure 9. Here the barotropic waves have two different meridional wave numbers, L_1 and L_2, so that the initial condition for the barotropic streamfunction can be written as

$$\psi_1=\delta^2\sin(L_1y)\frac{\beta_1}{\sqrt{2\pi L_1}}e^{i(k_{\mathrm{T}1}x-\omega_{\mathrm{T}1}t)}+\delta^2\sin(L_2y)\frac{\beta_2}{\sqrt{2\pi L_2}}e^{i(k_{\mathrm{T}2}x-\omega_{\mathrm{T}2}t)}+\mathrm{C.C.}\tag{23}$$

where β_1 and β_2 are the amplitudes for the two barotropic Rossby waves. The initial condition for the baroclinic system is

$$\vec{U}_1=\alpha(T_1,T_2)e^{i(k_{\mathrm{MJO}}x-\omega_{\mathrm{MJO}}t)}\vec{r}_{\mathrm{MJO}}+\vec{r}_{\mathrm{W}1}++\vec{r}_{\mathrm{W}2}+\mathrm{C.C.},\tag{24}$$

where $\vec{r}_{\mathrm{W}1}$ and $\vec{r}_{\mathrm{W}2}$ are the Walker circulation components at wave numbers $k_{\mathrm{W}}=2$ and 3. These two resonant triads lead to the reduced ODE system:

$$\partial_{T_2}\beta_1 \qquad\qquad\qquad +id_{21}\beta_1+h_{31}\alpha^*=0,\tag{25a}$$

$$\partial_{T_2}\beta_2 \qquad\qquad\qquad +id_{22}\beta_2+h_{32}\alpha^*=0,\tag{25b}$$

$$\partial_{T_2}\alpha+id_4\alpha^2\alpha^*+id_5\alpha+h_{61}{\beta_1}^*+h_{62}{\beta_2}^*=0.\tag{25c}$$

The derivation, not shown here, is similar to Chen et al. (2015). From system (25), we can see that both barotropic waves are interacting with the MJO mode (α), but there is no direct interaction between the two barotropic Rossby waves.

In principle, either one of the barotropic waves can potentially initiate the MJO. To consider each wave separately, two cases are computed numerically: (i) $\alpha|_{T_2=0}=0$, $\beta_1|_{T_2=0}=1$, $\beta_2|_{T_2=0}=0$, and (ii) $\alpha|_{T_2=0}=0$, $\beta_1|_{T_2=0}=0$, $\beta_2|_{T_2=0}=1$. The results, not shown here, show reasonable MJO initiation for the former case and weak MJO initiation for the latter case. Furthermore, additional cases, such as investigations of MJO termination, were also carried out. The results, not shown here, demonstrate that the energy transfer with the MJO is mainly contributed from that of the barotropic Rossby wave with $k_{\mathrm{T}}=1$, and the wavenumber $k_{\mathrm{T}}=2$ Rossby wave exchanges only a very small amount of energy with the MJO. It is possible that the meridional wavelength $\frac{2\pi}{L_2}$, which is ≈ 840 km is too small to initiate the MJO.

b. MJO–MJO–b.t. Rossby–b.t. Rossby

In this section, four modes are considered: the MJO modes with wavenumbers $k_{\mathrm{MJO}1}=1$, and $k_{\mathrm{MJO}2}=2$, and two barotropic Rossby waves with the same zonal wavenumbers $k_{\mathrm{T}1}=k_{\mathrm{T}2}=1$ but different meridional wavenumbers L_1 and L_2. Figure 10 shows the resonance condition for the interactions between the four modes. The ansatz for the barotropic wind can still be written as (23), and

$$\vec{U}_1=\alpha_1(T_1,T_2)e^{i(k_{\mathrm{MJO}1}x-\omega_{\mathrm{MJO}1}t)}\vec{r}_{\mathrm{MJO1}}+\alpha_2(T_1,T_2)e^{i(k_{\mathrm{MJO}2}x-\omega_{\mathrm{MJO}2}t)}\vec{r}_{\mathrm{MJO2}}+\vec{r}_{\mathrm{W1}}+\vec{r}_{\mathrm{W2}}+\mathrm{C.C.}, \tag{26}$$

for the baroclinic modes, where α_1 and α_2 stand for amplitudes for the MJO at wavenumbers $k_{\mathrm{MJO}1}=1$ and $k_{\mathrm{MJO}2}=2$. The following coupled ODE system describes the interaction mechanism:

$$\partial_{T_2}\beta_1 \qquad\qquad\qquad\qquad\qquad + id_{21}\beta_1 + h_{31}\alpha_1^* = 0, \tag{27a}$$

$$\partial_{T_2}\alpha_1 + id_{41}{\alpha_1}^2\alpha_1^* + ig_1\alpha_1\alpha_2\alpha_2^* + id_{51}\alpha_1 + h_{61}\beta_1^* = 0, \tag{27b}$$

$$\partial_{T_2}\beta_2 \qquad\qquad\qquad\qquad\qquad + id_{22}\beta_2 + h_{32}\alpha_2^* = 0, \tag{27c}$$

$$\partial_{T_2}\alpha_2 + id_{42}{\alpha_2}^2\alpha_2^* + ig_2\alpha_2\alpha_1\alpha_1^* + id_{52}\alpha_2 + h_{62}\beta_2^* = 0. \tag{27d}$$

Again, the derivation, not shown here, is similar to Chen et al. (2015). In this ODE system, besides the existing coupled linear terms between the MJO–barotropic Rossby wave interactions, additional cubic interactions appear between the two MJO modes. Specifically, the terms for MJO–MJO interactions are $ig_1\alpha_1\alpha_2\alpha_2^*$ in (27b) and $ig_2\alpha_2\alpha_1\alpha_1^*$ in (27d). These cubic interactions arise from the nonlinear *q*-*a* interaction in the MJO skeleton model, similar to the cubic self-interaction terms in Chen et al. (2015).

Figure 11 shows the MJO initiation with initial conditions $\alpha_1|_{T_2=0} = \alpha_2|_{T_2=0} = 0$ and $\beta_1|_{T_2=0} = \beta_2|_{T_2=0} = 1$. It can be seen from the reduced system (25) that the barotropic Rossby waves β_1 and β_2 are necessary to initiate MJO modes, α_1 and α_2, respectively. In Figure 11, the two MJO modes interact with each other, and the solutions are not following a periodic pattern. Also, notice that the MJO is significantly weakened for times 110-140 days, but it is not completely terminated. To illustrate this more clearly, Figure 12 is the Hovmoller diagram for the convective envelope of the leading order MJO waves with wave numbers 1 and 2. A wave packet is presented in the diagram that propagating westward at about 10 m/hr with a life cycle around 150 day. These cases illustrate additional realism, such as MJOs with more realistic zonal variations, through the interaction with the Walker circulation, with more realistic zonal variations.

5. Effects of wind shear

This section includes the effect of the horizontal and vertical wind shear in the model. We consider both the barotropic and baroclinic wind shear is $O(\delta^2)$:

$$(\tilde{u}(x,y,z),\tilde{v}(x,y,z),\tilde{w}(x,y,z)) = \left(\tilde{U}(y,z),0,0\right) \tag{28}$$

where

$$\tilde{U}(y,z) = \delta^2\left[U_0 + L\sin(Ly)B_0 + \cos(\pi z)\left(u^{(0)}{}_0\Phi_0 + u^{(2)}{}_0\Phi_2\right)\right]. \tag{29}$$

Here U_0 is the constant global mean flow, B_0 is the strength of the barotropic wind shear on the meridional direction, and $u^{(0)}{}_0$, $u^{(2)}{}_0$ are the strengths of the baroclinic wind shear on both vertical and meridional directions.

A similar multi-scale analysis is carried out, and the resonance condition is not affected by the wind shear. The reduced ODE model for the MJO–barotropic Rossby wave interaction is:

$$\partial_{T_2}\beta \qquad\qquad + i(d_2+f_1)\beta + h_3\alpha^* = 0 \tag{30a}$$

$$\partial_{T_2}\alpha + id_4\alpha^2\alpha^* + i(d_5+f_2)\alpha + h_6\beta^* = 0 \tag{30b}$$

The wind shear introduces two additional linear terms with coefficients f_1 and f_2, both of which are real values. In the derivation of these two linear terms, only the barotropic shear is involved. In order for the baroclinic shear to have an effect, it must instead be assumed to have an amplitude of $O(\delta)$; in such a case (not shown), it is noticed that the inclusion of the baroclinic shear also introduces similar self-interacting linear terms, so that the reduced ODE is in the same form of (30).

Numerical simulations are performed for MJO initiation with the effects of barotropic shear. The resonance condition is the same as in Section 3. Four different barotropic shear profiles are considered. (i) $U_0 = 0$, $B_0 = 1$, (ii) $U_0 = -1$, $B_0 = 1$, (iii) $U_0 = 1$, $B_0 = 0$, and (iv) $U_0 = 1$, $B_0 = 1$. The results for the four cases are recorded in Table 2, which lists the value for the coefficients f_1 and f_2, the maximum amplitude attained by MJO and the time period of the solution. From the table, we notice that the shear does not significantly affect the energy exchange between the MJO and the barotropic Rossby waves.

6. Concluding discussion

Asymptotic models have been designed and analyzed here for the nonlinear interaction between the MJO and the barotropic Rossby waves. The models involve the combination of the barotropic and equatorial baroclinic modes together with interactive moisture and convective activity envelope. An important feature of this framework is that the tropical and extratropical dynamics are interactive, rather than specifying one of these components as an external forcing term or boundary condition.

To explore more realistic conditions, Walker circulations were also considered with more general zonal variations. With the presence of the Walker circulation, the MJO and the barotropic Rossby waves can interact directly. In Section 3, the reduced ODE model is derived by identifying resonant triads that include: the MJO, the Walker circulation, and the barotropic Rossby wave. Two cases are presented: (i) MJO initiation, and (ii) MJO termination and excitation of barotropic Rossby waves. In contrast to the results in Chen et al. (2015), where the barotropic Rossby wave exchanges very little energy with other modes, here with the Walker circulation, the barotropic Rossby wave and the MJO are exchanging energy directly. The time period between initiation and termination is about 140 days, a realistic timescale which corresponds to one or two MJO events, depending on the spatial location.

To explore more realistic conditions, Walker circulations were also considered with more general zonal variations. More resonant triads are identified to generate energy exchange between different modes. In particular, a four wave MJO–MJO–barotropic Rossby–barotropic Rossby interaction is found with MJO at wave numbers 1 and 2, where the two MJO modes are interacting through the nonlinear coupling term between moisture and convective activity envelope in the MJO skeleton equation. In this case, rather than an idealized MJO with a single zonal wavenumber, a wave packet of MJO events arises with an amplitude that is zonally localized.

As a final element of additional realism considered here, horizontal and vertical shear were incorporated in the model. From our model, the barotropic and baroclinic shear, if zonally uniform, have little effect on the energy exchange between the MJO and the barotropic Rossby waves. This is in contrast to the significant effect of zonally varying wind shear as part of the Walker circulation. Further investigations are needed to better understand the role of wind shear in these different settings.

While this simplified asymptotic model includes several realistic aspects of tropical–extratropical interactions, some other physical mechanisms are not included. For instance, the meridional structures of the variables here are set to be the leading parabolic cylinder functions. With more complicated meridional structures, the interaction mechanism will be richer and more realistic, and it would allow the model to cope with different background states, such as the boreal summer/winter, when the ITCZ is off the equator. Such topics are interesting avenues for future investigations.

Acknowledgments. The research of A.J.M. is partially supported by Office of Naval Research grant ONR MURI N00014-12-1-0912. The research of S.N.S. is partially supported by Office of Naval Research grant ONR MURI N00014-12-1-0912, ONR Young Investigator Award ONR

N00014-12-1-0744, National Science Foundation grant NSF DMS-1209409, and a Sloan Research Fellowship. S.C. is supported as a postdoctoral research associate by the ONR grants.

APPENDIX

Asymptotic expansion of the meridional truncated system

The parabolic cylinder functions that are used to define the meridional structure of the baroclinic variables are:

$$\Phi_m(y) = \left(m!\sqrt{\pi}\right)^{-\frac{1}{2}} 2^{-\frac{m}{2}} e^{-\frac{y^2}{2}} H_m(y), \tag{A1}$$

with Hermite polynomials $H_m(y)$ defined by

$$H_m(y) = (-1)^m e^{y^2} \frac{d^m e^{-y^2}}{dy^m}. \tag{A2}$$

The parabolic cylinder functions form an orthonormal basis on the 1D function space. The first few functions are

$$\Phi_0(y) = \pi^{-\frac{1}{4}} e^{-y^2/2}, \quad \Phi_1(y) = \pi^{-\frac{1}{4}} \sqrt{2} y e^{-y^2/2}, \quad \Phi_2(y) = \pi^{-\frac{1}{4}} \frac{1}{\sqrt{2}} (2y^2 - 1) e^{-y^2/2}. \tag{A3}$$

The parabolic cylinder functions satisfy the following identities:

$$\mathscr{L}_+ \Phi_m(y) = (2m)^{1/2} \Phi_{m-1}(y), \quad \mathscr{L}_- \Phi_m(y) = -\left[2(m+1)\right]^{1/2} \Phi_{m+1}(y), \tag{A4}$$

which help to simplify many expressions, where the operators $\mathscr{L}_\pm$ are defined as $\mathscr{L}_\pm = \frac{\partial}{\partial y} \pm y$.

The equations (3) for the Walker circulation can be written for the truncated system as

$$-l^{(0)}{}_{1sx}+v^{(1)}{}_{1s}+\frac{1}{\sqrt{2}}\bar{H}a^{(0)}{}_{1s}=\frac{1}{\sqrt{2}}c_q\tilde{S}^x, \tag{A5a}$$

$$-l^{(2)}{}_{1sx}=0, \tag{A5b}$$

$$r^{(0)}{}_{1sx}+\frac{1}{\sqrt{2}}\bar{H}a^{(0)}=\frac{1}{\sqrt{2}}c_q\tilde{S}^x, \tag{A5c}$$

$$r^{(2)}{}_{1sx}-\sqrt{2}v^{(1)}{}_{s1}=0 \tag{A5d}$$

$$-l^{(0)}{}_{1s}+\sqrt{2}r^{(2)}{}_{1s}=0, \tag{A5e}$$

$$\frac{\tilde{Q}}{\sqrt{2}}(r^{(0)}{}_{1sx}-l^{(0)}{}_{1sx})+\frac{\tilde{Q}}{\sqrt{2}}v^{(1)}{}_{1s}+\bar{H}a^{(0)}{}_{1s}=c_\theta\tilde{S}^x, \tag{A5f}$$

$$\frac{\tilde{Q}}{\sqrt{2}}(r^{(2)}{}_{1sx}-l^{(2)}{}_{1sx})-\tilde{Q}v^{(1)}{}_{1s}=0. \tag{A5g}$$

The solution to this system of equations is the Walker circulation in the meridional truncated system, and it can be written as

$$r^{(0)}{}_{1\mathrm{W}x}=-\frac{c_q-c_\theta}{\sqrt{2}(\tilde{Q}-1)}\tilde{S}^x, \tag{A6a}$$

$$l^{(0)}{}_{1\mathrm{W}x}=\frac{\sqrt{2}(c_q-c_\theta)}{\tilde{Q}-1}\tilde{S}^x, \tag{A6b}$$

$$r^{(2)}{}_{1\mathrm{W}x}=\frac{1}{\sqrt{2}}l^{(0)}{}_{1\mathrm{W}x} \tag{A6c}$$

$$v^{(1)}{}_{1\mathrm{W}}=\frac{1}{2}l^{(0)}{}_{1\mathrm{W}x}, \tag{A6d}$$

$$q^{(0)}{}_{1\mathrm{W}}=0, \tag{A6e}$$

$$a^{(0)}{}_{1\mathrm{W}}=\frac{\tilde{Q}c_q-c_\theta}{\bar{H}(\tilde{Q}-1)}\tilde{S}^x. \tag{A6f}$$

By writing the baroclinic variables as $\vec{U}=[l^{(0)},l^{(2)},r^{(0)},r^{(2)},v^{(1)},q^{(0)},q^{(2)}]$ for the truncated system, and writing $\vec{U}_1=\vec{U}_{1\mathrm{a}}+\vec{U}_{1\mathrm{W}}$ to separate the Walker circulation ($\vec{U}_{1\mathrm{W}}$) from the anomalies ($\vec{U}_{1\mathrm{a}}$), the asymptotic expansion of (1), (2), (8), (11) and (12) can be written in abstract form as follows. Expanding (1) and (2) in powers of δ, the first order system is

$$L^2 YB_{1t'} - YB_{1x'} = 0, \tag{A7a}$$

$$\mathcal{N}\vec{U}_{1at'} + \mathcal{L}_{\vec{U}}\vec{U}_{1a} = 0, \tag{A7b}$$

the second order system is

$$L^2 YB_{2t'} - YB_{2x'} = -L^2 YB_{1T_1}, \tag{A8a}$$

$$\mathcal{N}\vec{U}_{2t'} + \mathcal{L}_{\vec{U}}\vec{U}_2 = -\vec{U}_{1aT_1} + \vec{F}_{2\vec{U}_{1a}} + \vec{F}_{2\vec{U}_{1W}}, \tag{A8b}$$

and the third order system is

$$\begin{aligned} L^2 YB_{3t'} - YB_{3x'} = -L^2 YB_{1T_2} - L^2 YB_{2T_1} + YB_{1x'x't'} \\ + \mathscr{B}_{T3}(\vec{U}_{1a}, \vec{U}_{1a}) + \mathscr{B}_{T3}(\vec{U}_{1a}, \vec{U}_{1W}) + \mathscr{B}_{T3}(\vec{U}_{1W}, \vec{U}_{1W}), \end{aligned} \tag{A9a}$$

$$\mathcal{N}\vec{U}_{3t'} + \mathcal{L}_{\vec{U}}\vec{U}_3 = -\vec{U}_{1T_2} - \vec{U}_{2T_1} + \vec{F}_{3\vec{U}_2,\vec{U}_{1a}} + \vec{F}_{3\vec{U}_2,\vec{U}_{1W}} + \vec{\mathscr{B}}_3(B_1, \vec{U}_{1a}) + \vec{\mathscr{B}}_3(B_1, \vec{U}_{1W}). \tag{A9b}$$

Here $\mathcal{N} = \mathrm{diag}(1,1,1,1,0,1,1,1)$ is the 8×8 matrix where the '0' entry is to eliminate $\partial_t v^{(1)}$, $\vec{F}$ represents terms from the nonlinear interactions between q and a, and $\mathscr{B}$ represents the bilinear terms from the nonlinear interactions in the dry dynamics. The detailed descriptions for these terms can be found in Chen et al. (2015).

References

Chen, S., A. J. Majda, and S. N. Stechmann, 2015: Multiscale asymptotics for the skeleton of the Madden–Julian oscillation and tropical-extratropical interactions. *Mathematics of Climate and Weather Forescasting*, **1**, 43–69.

Ferranti, L., T. N. Palmer, F. Molteni, and E. Klinker, 1990: Tropical-extratropical interaction associated with the 30-60 day oscillation and its impact on medium and extended range prediction. *J. Atmos. Sci.*, **47 (18)**, 2177–2199.

Frederiksen, J. S., and C. S. Frederiksen, 1993: Monsoon disturbances, intraseasonal oscillations, teleconnection patterns, blocking, and storm tracks of the global atmosphere during January 1979: Linear theory. *J. Atmos. Sci.*, **50**, 1349–1372.

Gloeckler, L. C., and P. E. Roundy, 2013: Modulation of the extratropical circulation by combined activity of the Madden–Julian oscillation and equatorial Rossby waves during boreal winter. *Mon. Wea. Rev.*, **141**, 1347–1357.

Hoskins, B. J., and T. Ambrizzi, 1993: Rossby wave propagation on a realistic longitudinally varying flow. *J. Atmos. Sci.*, **50 (12)**, 1661–1671.

Hoskins, B. J., and F.-F. Jin, 1991: The initial value problem for tropical perturbations to a baroclinic atmosphere. *Q. J. R. Meteorol. Soc.*, **117**, 299–317.

Jin, F.-F., and B. J. Hoskins, 1995: The direct response to tropical heating in a baroclinic atmosphere. *J. Atmos. Sci.*, **52 (3)**, 307–319.

Khouider, B., and A. J. Majda, 2005: A non-oscillatory balanced scheme for an idealized tropical climate model: Part I: Algorithm and validation. *Theor. Comp. Fluid Dyn.*, **19 (5)**, 331–354.

Lau, W. K. M., and D. E. Waliser, Eds., 2012: *Intraseasonal Variability in the Atmosphere–Ocean Climate System*. Springer, Berlin.

Liebmann, B., and D. L. Hartmann, 1984: An observational study of tropical-midlatitude interactin on intraseasonal time scales during winter. *J. Atmos. Sci.*, **41 (23)**, 3333–3350.

Lin, H., G. Brunet, and J. Derome, 2009: An observed connection between the north Atlantic oscillation and the Madden–Julian oscillation. *J. Clim.*, **22**, 364–380.

Madden, R. A., and P. R. Julian, 1971: Detection of a 40–50 day oscillation in the zonal wind in the tropical Pacific. *J. Atmos. Sci.*, **28 (5)**, 702–708.

Madden, R. A., and P. R. Julian, 1972: Description of global-scale circulation cells in the Tropics with a 40–50 day period. *J. Atmos. Sci.*, **29**, 1109–1123.

Madden, R. A., and P. R. Julian, 1994: Observations of the 40–50-day tropical oscillation—a review. *Mon. Wea. Rev.*, **122**, 814–837.

Majda, A. J., and J. A. Biello, 2003: The nonlinear interaction of barotropic and equatorial baroclinic Rossby waves. *J. Atmos. Sci.*, **60**, 1809–1821.

Majda, A. J., and R. Klein, 2003: Systematic multiscale models for the Tropics. *J. Atmos. Sci.*, **60**, 393–408.

Majda, A. J., R. R. Rosales, E. G. Tabak, and C. V. Turner, 1999: Interaction of large-scale equatorial waves and dispersion of kelvin waves through topographic resonances. *J. Atmos. Sci.*, **56**, 4118–4133.

Majda, A. J., and S. N. Stechmann, 2009: The skeleton of tropical intraseasonal oscillations. *Proc. Natl. Acad. Sci. USA*, **106 (21)**, 8417–8422.

Majda, A. J., and S. N. Stechmann, 2011: Nonlinear dynamics and regional variations in the MJO skeleton. *J. Atmos. Sci.*, **68**, 3053–3071.

Matthews, A., B. J. Hoskins, and M. Masutani, 2004: The global response to tropical heating in the Madden–Julian oscillation during the northern winter. *Q. J. R. Meteorol. Soc.*, **130**, 1991–2011.

Matthews, A., and G. N. Kiladis, 1999: The tropical–extratropical interaction between high-frequency transients and the Madden–Julian oscillation. *Mon. Wea. Rev.*, **127**, 661–677.

Ogrosky, H. R., and S. N. Stechmann, 2015: The MJO skeleton model with observation-based background state and forcing. *Quarterly Journal of the Royal Meteorological Society*, **141**, 2654–2669.

Ray, P., and C. Zhang, 2010: A case study of the mechanics of extratropical influence on the initiation of the Madden–Julian oscillation. *J. Atmos. Sci.*, **67**, 515–528.

Roundy, P. E., 2011: Tropical–extratropical interactions. *Intraseasonal Variability in the Atmosphere–Ocean Climate System*, W. K. M. Lau, and D. E. Waliser, Eds., Springer, Berlin.

Stechmann, S. N., and A. J. Majda, 2015: Identifying the skeleton of the madden–julian oscillation in observational data. *Monthly Weather Review*, **143 (1)**, 395–416.

Stechmann, S. N., and H. R. Ogrosky, 2014: The Walker circulation, diabatic heating, and outgoing longwave radiation. *Geophysical Research Letters*, **41 (24)**, 9097–9105.

Thual, S., A. J. Majda, and S. N. Stechmann, 2014: A stochastic skeleton model for the MJO. *J. Atmos. Sci.*, **71**, 697–715.

Webster, P. J., 1972: Response of the tropical atmosphere to local steady forcing. *Mon. Wea. Rev.*, **100**, 518–541.

Webster, P. J., 1981: Mechanisms determining the atmospheric response to sea surface temperature anomalies. *J. Atmos. Sci.*, **38**, 554–571.

Webster, P. J., 1982: Seasonality in the local and remote atmospheric response to sea surface temperature anomalies. *J. Atmos. Sci.*, **39**, 41–52.

Weickmann, K. M., 1983: Intraseasonal circulation and outgoing longwave radiation modes during northern hemisphere winter. *Mon. Wea. Rev.*, **111**, 1838–1858.

Weickmann, K. M., and E. Berry, 2009: The tropical Madden–Julian oscillation and the global wind oscillation. *Mon. Wea. Rev.*, **137**, 1601–1614.

Weickmann, K. M., G. R. Lussky, and K. J. E., 1985: Intraseasonal (30-60 day) fluctuations of outgoing longwave radiation and 250 mb streamfunctin during northern winter. *Mon. Wea. Rev.*, **113**, 941–961.

Yoneyama, K., C. Zhang, and C.-N. Long, 2013: Tracking pulses of the Madden-Julian oscillation. *Bull. Amer. Meteor. Soc.*, **94**, 1871–1891.

Zhang, C., 2005: Madden–Julian Oscillation. *Reviews of Geophysics*, **43**, RG2003, doi:10.1029/2004RG000158.

LIST OF TABLES

c_q	h_3	h_6
1.2	-0.13	0.41
1.1	-0.06	0.21
1	0	0
0.9	0.06	-0.21
0.8	0.13	-0.41

TABLE 1. Coefficients in the reduced ODE system (18) with different values of c_q, and $c_\theta = 1$. See (14) for the definitions of parameters c_q and c_θ.

U_0	B_0	f_1	f_2	$\max\|\alpha\|$	Time period (day)
0	1	0	6.6e-2	1.80	147
-1	1	0.15	7.7e-3	1.79	147
1	0	-0.15	0.06	1.70	135
1	1	-0.15	0.12	1.76	141

TABLE 2. Coefficients f_1 and f_2 for the linear terms in (30). Also shown are the MJO amplitude and oscillation period for the nonlinear solutions (30) for different values of the barotropic shears U_0 and B_0, which are defined in (29).

LIST OF FIGURES

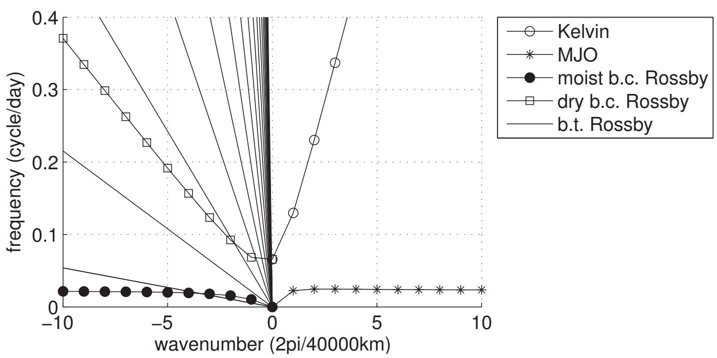

517 FIG. 1. Dispersion relation for linear waves. The dispersion curve of the Kelvin mode is denoted as open circles, the MJO as asterisks, the moist baroclinic Rossby mode as closed circles, the dry baroclinic Rossby mode as squares, and the barotropic Rossby mode with no symbols.

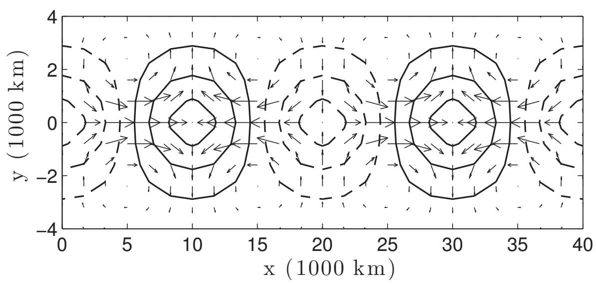

520 FIG. 2. Walker circulation with wavenumber $k_W = 2$. The contours denote the convective activity $\bar{H}a$, with positive (negative) anomalies denoted by solid (dashed) contours and with the zero contour removed. The contour interval is equal to one-fourth of the maximum value of $\bar{H}a$. The vectors denote the horizontal velocity field at the lower troposphere.

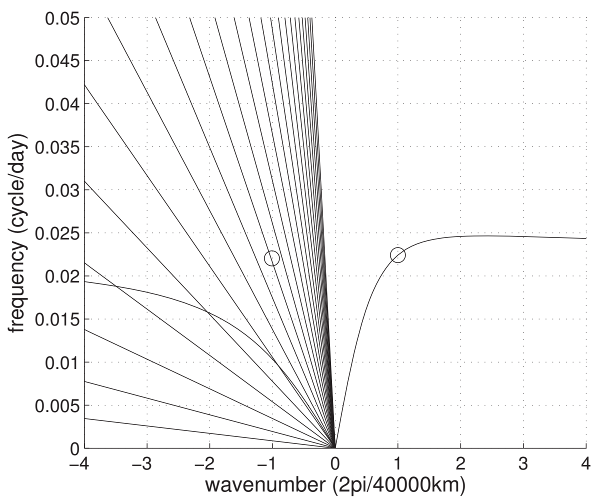

524 FIG. 3. Resonance condition for the interaction of the MJO, Walker circulation, and barotropic Rossby wave

525 with wavenumbers $k_{\mathrm{MJO}} = 1$, $k_{\mathrm{W}} = -2$ and $k_{\mathrm{T}} = 1$ as described in (15).

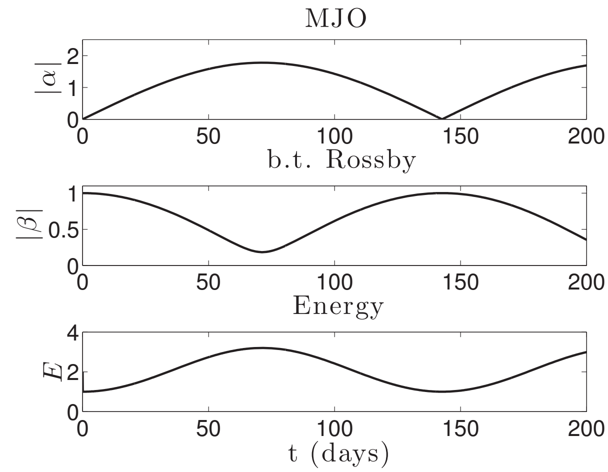

FIG. 4. Solution of the reduced model (18) for the case of MJO initiation with $k_{\mathrm{MJO}} = 1$, $k_{\mathrm{W}} = -2$ and $k_{\mathrm{T}} = 1$.

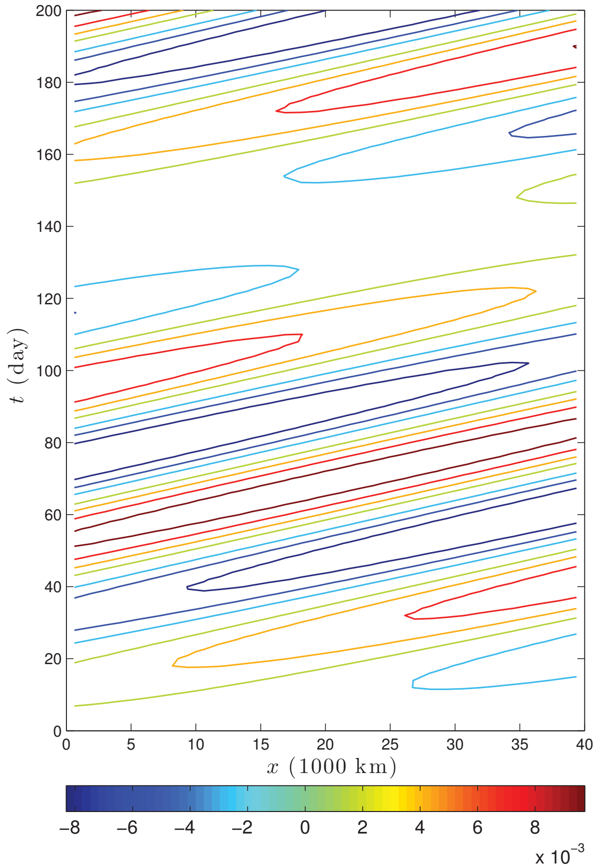

FIG. 5. Hovmoller diagram of $\bar{H}a_{1\mathrm{a}}$ convective activity for the case of MJO initiation.

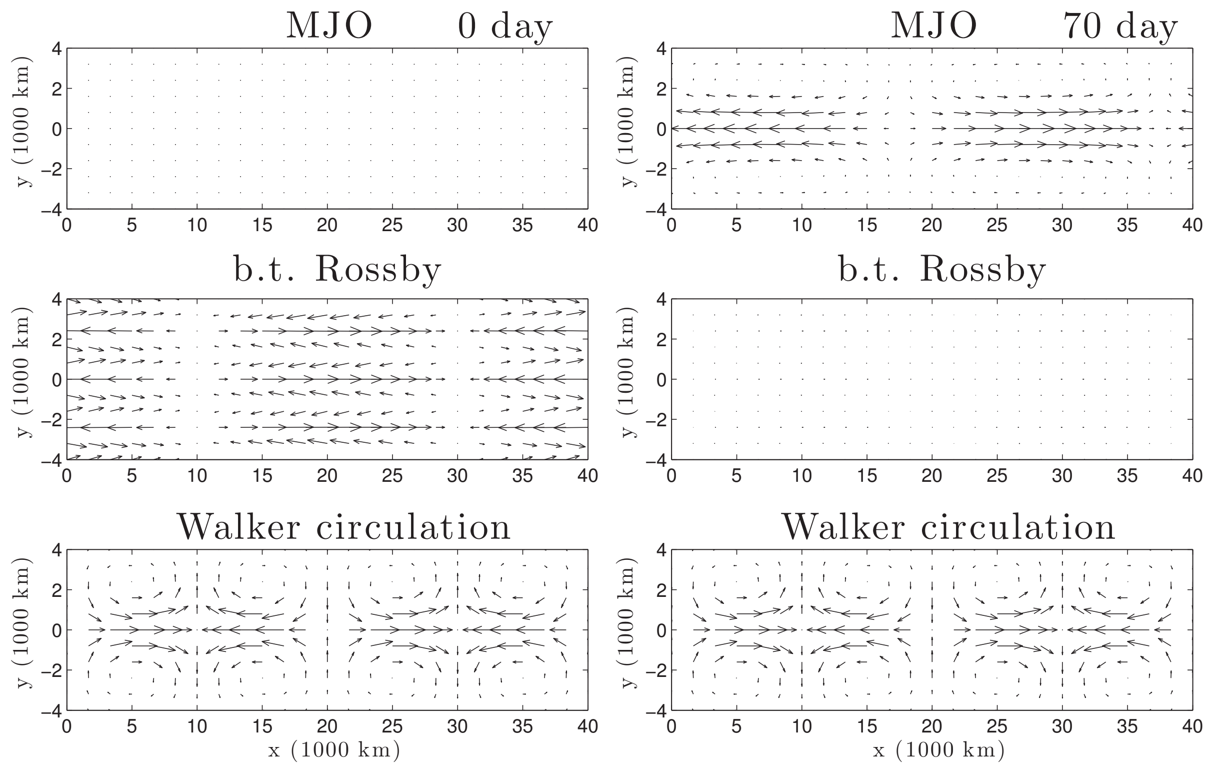

526 FIG. 6. Velocity field (lower-tropospheric) of three modes for the case of MJO initiation. Left: at 0 day; right:
527 at 70 day. Top row: MJO. Middle row: barotropic Rossby wave. Bottom row: Walker circulation.

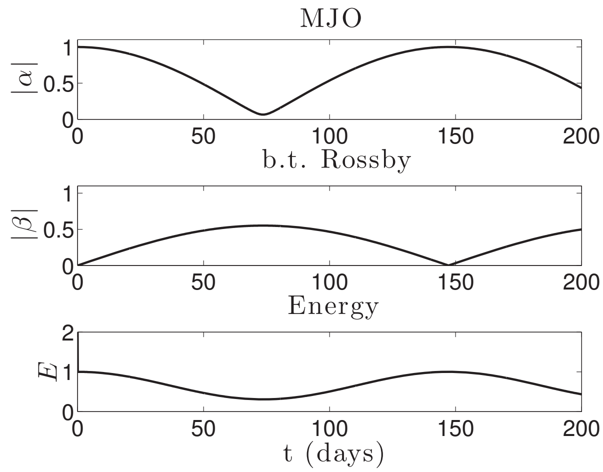

528 FIG. 7. As in Figure **??**, but with initial conditions corresponding to the case of MJO termination and excitation of barotropic Rossby wave.

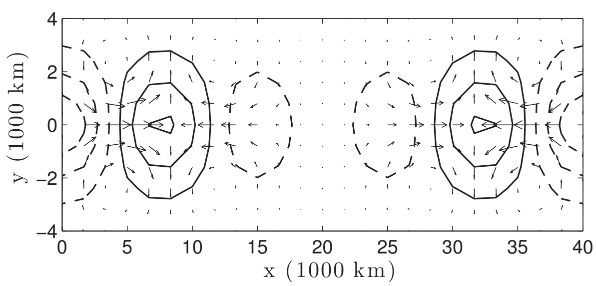

FIG. 8. As in Figure 2, but for a Walker circulation with wavenumbers $k_{\mathrm{W}} = 2$ and 3 as described in Section 4.

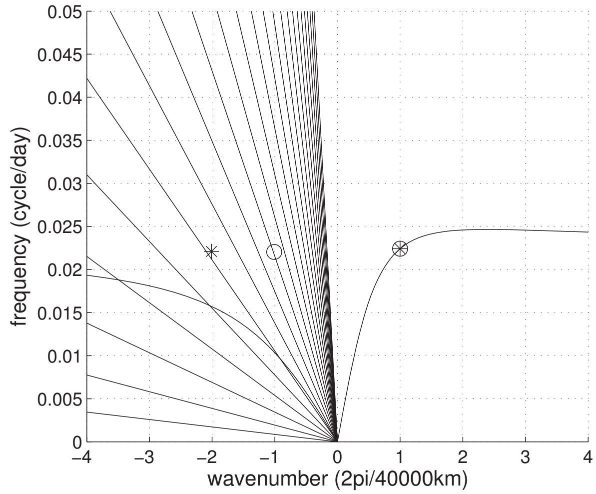

530 FIG. 9. Resonance conditions (21)-(22) with more realistic Walker circulation with one MJO mode as de-
531 scribed in Section 4a. Open circles correspond with (21) and asterisks correspond with (22).

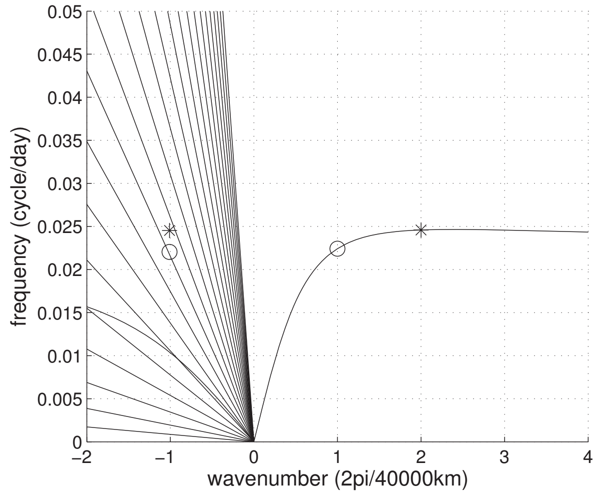

FIG. 10. Same as Figure 9, but for the case with two MJO modes, as described in Section 4b.

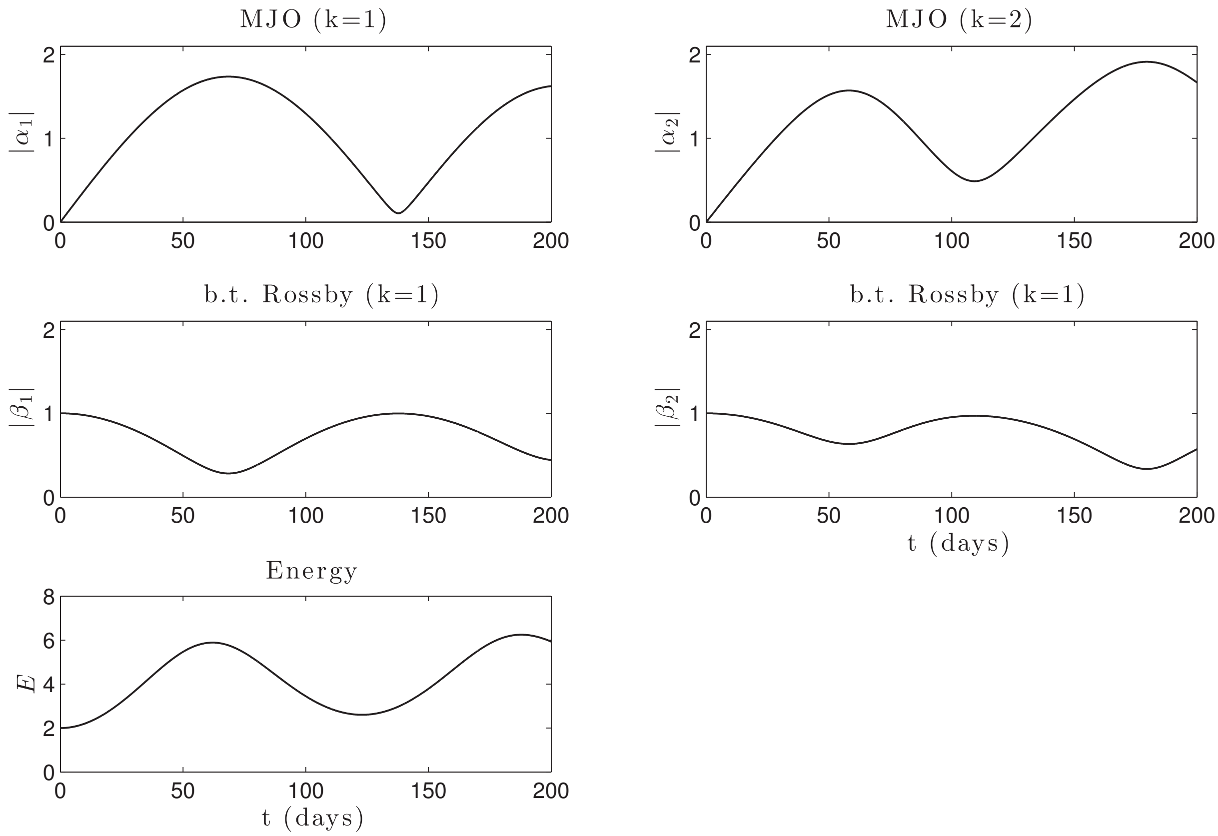

532 FIG. 11. Solution of the reduced model (27) for the case of MJO initiations with two MJO modes: $k_{\mathrm{MJO}1} = 1$
533 and $k_{\mathrm{MJO}2} = 2$ as described in Section 4b.

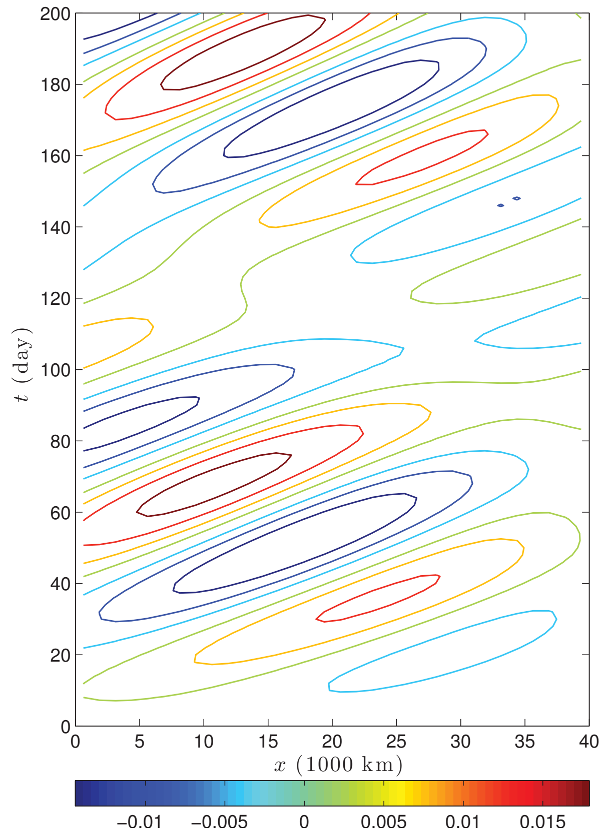

FIG. 12. Hovmoller diagram of $\bar{H}a_{1\mathrm{a}}$ for MJO initiation with two MJO modes: $k_{\mathrm{MJO}1} = 1$ and $k_{\mathrm{MJO}2} = 2$ as described in Section 4b.